ELSEVIER

Thin Solid Films 401 (2001) 284–290

thin solid films

www.elsevier.com/locate/tsf

Spectroscopic impedance studies of Al_2O_3 films deposited by spray pyrolysis

A. Huanosta*, J.C. Alonso, A. Ortiz

Instituto de Investigaciones en Materiales, UNAM, Coyoacán, 04510 Mexico D.F., A.P. 70-360, Mexico

Received 23 September 2000; received in revised form 28 August 2001; accepted 17 September 2001

Abstract

Alternating current (AC) experiments have been carried out from room temperature up to 500 °C in order to obtain dielectric properties of Al_2O_3 amorphous films deposited by ultrasonic spray pyrolysis. Temperature-dependent complex impedance of the films studied results in classically shaped spectra. Up to 300 °C, this shows a single relaxation process described by a non-largely depressed semicircle, as in single-phase material. Above this temperature, a second relaxation process arises due to spatial charge accumulation in the vicinity of the electrode region. Bulk electric characteristics were determined proposing equivalent circuits constituted by resistive (R) and capacitive (C) elements. A current-fitting routine has permitted an acceptable calculation of these parameters. The dielectric constant was determined as a function of the temperature and frequency and it was found to be constant for a wide range of frequencies. The dependence on frequency and temperature of the total $\sigma_t(\omega,T)$ conductivity was also investigated. The temperature dependence of $\sigma_t(\omega,T)$ shows a wide region where it is almost temperature-independent. Using frequency-dependent conductivity results, it was established that a jump-charge carrier mechanism is the principal responsible for electrical conductivity in these films. This mechanism involves both electronic and ionic charge carriers, and follows the Jonscher power law, $\sigma_t(\omega,T)=\sigma_0+A\omega^s$. We report the temperature dependence of the A and s parameters. © 2001 Elsevier Science B.V. All rights reserved.

Keywords: Pyrolysis; Spectroscopic impedance; Equivalent circuit; Frequency-dependent conductivity; Ionic charge carriers

1. Introduction

Insulator thin films are currently used in different electronic devices. The functional characteristics required for the insulators depend on their specific application. For example, the insulator films used in alternating-current thin-film electroluminescent (ACTFEL) devices, such as metal–insulator–semiconductor–insulator–metal (MISIM) structures [1], must have both high electric-field strength (E_b) to withstand the voltage pulses applied to the structure and high dielectric constant (ε') to reduce the threshold operation voltage. These are stringent requirements for the insulators, since E_b and ε' are commonly inversely proportional to each other. Another aspect that must be taken into account for the application of insulator films in this type of device is their electrical response as a function of the frequency of the applied voltage, as well as their stability under different working conditions (temperature, humidity, etc.). Various oxides, such as Al_2O_3, Y_2O_3, TiO_2, HfO_2, Ta_2O_5 and SiO_2, have been used as insulators in ACTFEL devices with the aim of finding the most suitable insulator for this application [1–7]. However, most of these studies have been devoted to characterizing the efficiency of the electroluminescent devices and/or the charge transfer mechanisms, mainly focussing on the properties of the semiconductor active layer and the insulator–semiconductor interface. The spectral dielectric response of these insulator films is commonly preassumed and/or it is only implicitly studied as a part of the complete electroluminescent device, but to our

* Corresponding author.
E-mail address: huanosta@servidor.unam.mx (A. Huanosta).

PII: S0040-6090(01)01621-2

knowledge it has been scarcely evaluated in a separate way. The aim of the present work is to characterize the frequency and temperature dependence of the dielectric properties of aluminum oxide (Al_2O_3) films deposited by spray pyrolysis, which have been recently used as insulating films in ACTFEL devices [8].

There are a number of formalisms that can be used for characterizing dielectric and/or electric properties of insulators [9]. The most frequently used methods [10] for analyzing electrical properties as a function of frequency are: impedance (Z^*); admittance [$Y^* = (Z^*)^{-1}$]; relative permittivity [$\varepsilon^* = (j\omega C_0 Z^*)^{-1}$]; and electric modulus [$M = (\varepsilon^*)^{-1}$]. An appropriate choice would emphasize particular aspects of the electrical response from a system. In this study, we have selected the complex impedance spectroscopy technique for analyzing the electrical response of spray pyrolysis-deposited Al_2O_3 films. Impedance spectroscopy studies have been previously carried out on several types of composite solid electrolytes incorporating Al_2O_3 [11,12]; however, these studies have been scarcely applied to study amorphous Al_2O_3 films, and in these cases the films have been obtained by techniques different to that used in this work [13,14].

2. Experimental

The Al_2O_3 films were deposited by the ultrasonic spray pyrolysis technique. The apparatus used for deposition has been described earlier [15]. It basically consists of an ultrasonic atomization chamber linked to the pyrolysis reactor by a transport nozzle. The substrate temperature was 480 °C. The starting solution was 0.05 M aluminum acetylacetonate (AlAcAc, Aldrich) dissolved in one part of high-purity methanol and three parts of deionised water, with the subsequent addition of 3 ml of acetic acid per liter of this solution. In order to determine the electrical characteristics of the films, they were deposited onto Pyrex glass coated with an antimony-doped tin oxide transparent conductive layer. A small part of the substrate was covered during deposition with a cover glass slide, to allow deposition of a metallic electrode. Aluminum contacts were thermally evaporated onto the Al_2O_3 films to fabricate the metal/oxide/metal structures needed for the electrical measurements. A mask was used to produce aluminum dots with an area of 0.352 cm^2.

The sandwich configuration used here is similar to that observed in EL devices of the MISIM type, where an insulating film is deposited onto a transparent conductive contact.

The composition, structural, optical and DC electrical properties of these films have been reported elsewhere [16]. The films in the present study have the following characteristics: (1) amorphous; (2) oxygen-rich, O/Al ratio of 1.74; (3) resistivity $\rho \cong 10^{14}$ Ω cm; (4) refractive index $n = 1.647$; and (5) bandgap wider than 6.2 eV. The thickness of the films deposited was measured by means of a Dektac IIA profilometer, having values of the order of 150 nm.

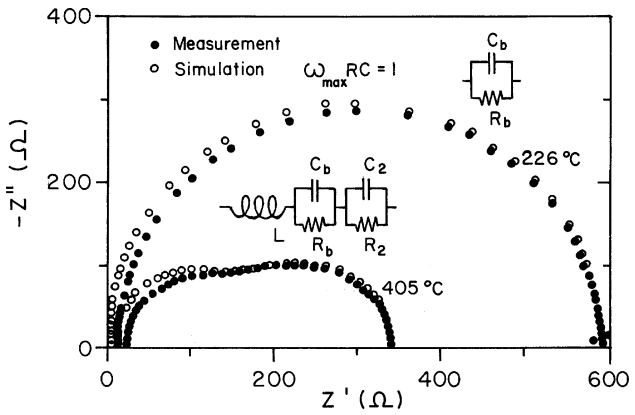

Fig. 1. Experimental and simulated impedance data at selected temperatures. A single semicircle is observed at low temperatures, while two arcs can be distinguished at high temperatures. Equivalent circuits are also included.

In order to perform the AC experiments, films were placed in a normal electrical furnace. Pt wires were used as contacts between the metallic electrodes deposited and the measurement device. A chromel–alumel thermocouple placed close to the sample (3–4 mm) was used to detect the several set temperatures, which have an associated error of ±3 °C. The AC measurements were performed in the frequency range from 5 to 13 MHz, using a Hewlett-Packard HP4192A automatic impedance analyzer controlled by a PC microcomputer. The temperature interval investigated was from room temperature up to 500 °C. Measurements were carried out every 30 min in order to guarantee thermal equilibrium conditions in the films studied. The applied voltage was 1 V.

3. Results

The general characteristics of the data from impedance experiments were as follows. At room temperature, it was not possible to obtain any electrical response from the films. Identifiable experimental information on impedance plots were only obtained above 150 °C. At this temperature, an incipient arc appears at the impedance plane; however, for temperatures from 200 up to 340 °C, well-formed single semicircles are observed. Above 340 °C, a second semicircle appears in the impedance plane in the low-frequency region. Fig. 1 shows the impedance spectra for two selected temperatures, 226 and 405 °C, where both previously mentioned behaviors are clearly evident. Both curves show a shift from the origin of co-ordinates of the high-frequency response, which becomes larger at higher temperatures.

This shift is related to a small impedance contribution from the instrument and leads. The impedance analysis was performed for those frequencies on the resultant curves where only dielectric properties of the film determine the impedance spectra, which define the corresponding dielectric window. Deviation from Debye ideality was also observed in the full circular arcs. This type of response commonly occurs in a single-phase ceramic material, but more frequently in glass or in disordered solids.

The impedance spectrum for 226 °C, shown in Fig. 1, is composed of a single arc, which indicates that a single relaxation process is occurring in the film. Therefore, in this case it is possible to use a simple parallel *RC*-equivalent circuit to simulate the electrical response, where *R* and *C* are discrete elements to be determined from the impedance expression:

$$Z^* = \left[(1/R_b) + j\omega C_b\right]^{-1} \quad (1)$$

where ω is the angular frequency and $j = \sqrt{-1}$. The subscript b for parameters *R* and *C* in Eq. (1) denotes that they describe bulk properties, as will be shown later. As is well known, the value of R_b is given by the diameter of the semicircle and C_b can be determined [17] from the relation $\omega_{max} R_b C_b = 1$, which holds at the semicircle maximum.

Above 340 °C, for instance at 405 °C in Fig. 1, the impedance data can be simulated by two parallel *RC* circuits connected in series. The associated impedance is given by:

$$Z^* = \left[(1/R_b) + j\omega C_b\right]^{-1} + \left[(1/R_2) + j\omega C_2\right]^{-1} \quad (2)$$

where the parallel R_2C_2 circuit characterizes the second semicircle.

The evaluation of the *R* and *C* elements was made both by direct calculation from the impedance plots, and by the use of the NLLS fitting routine by Boukamp [18]. The latter was performed in order to obtain reliable calculations. Discrepancy between both procedures was less than 4 and 8% for *R* and *C*, respectively. Nevertheless, this is not an evaluation of experimental uncertainty, it is rather a consequence of manipulation of the apparent geometry on the impedance curves. Above 340 °C and at high frequencies, impedance curves show strong dispersion of the imaginary component, as if an inductive component were involved. Since this effect cannot be explained in terms of the physical behavior of the film, it can be attributed to the external circuit, as suggested in [19]. Thus, inductive elements were considered only to simulate experimental curves above 340 °C. The fitting of the simulated and experimental data in this case is illustrated in Fig. 1 for 405 °C.

Using the *R* values calculated and transforming them to conductivity through the formula $\sigma_b = g/R$, where *g* (=film thickness/area of one electrode) is a geometrical factor, the dependence of the bulk conductivity on temperature was determined. Fig. 2a shows this dependence for σ_b values calculated from both plots exhibiting a single semicircle ($T < 340$ °C), and plots with two semicircular arcs ($T > 340$ °C). It is widely accepted [20] that the high-frequency response is associated with bulk properties when an appropriate (~1–100 pF) capacitance value is found. Values of C_b from the films studied were found to fulfill this requisite at the high-frequency arc.

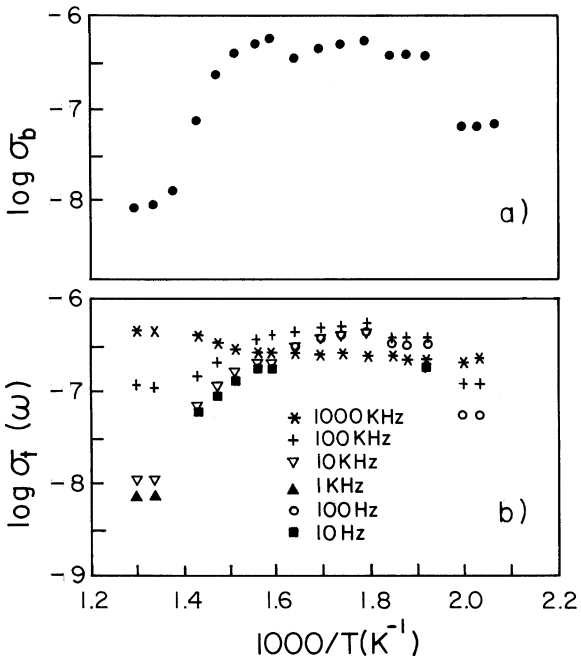

Fig. 2. Temperature dependence of conductivity: (a) bulk conductivity; and (b) dynamic conductivity plotted at selected frequencies.

An almost temperature-independent bulk conductivity behavior can be observed from 250 to approximately 400 °C. As a consequence, quite a small activation energy is involved ($\cong 0.06 \pm 0.003$ eV), while at temperatures above 400 °C, the bulk conductivity decreases. This stage corresponds to the development of the two semicircles on the impedance plane.

Additional characteristics of the frequency and temperature dependence of the conductivity can be found by working out the total $\sigma_t(\omega,T)$ conductivity, given by:

$$\sigma_t(\omega,T) = gZ'/\left[(Z')^2 + (Z'')^2\right] \quad (3)$$

where Z' and Z'' are the real and imaginary components of the complex impedance, respectively.

The temperature dependence of $\sigma_t(\omega,T)$ is shown in Fig. 2b. These plots were constructed by selecting data at the frequencies 0.01, 0.1, 1, 10 and 100 kHz and 1 MHz. None of these curves follows a linear behavior. Conductivity dispersion due to relaxation effects can be observed through all frequencies; furthermore, curves for the highest (100 kHz, 1 MHz) frequencies exhibit additional dispersion due to the inductive component

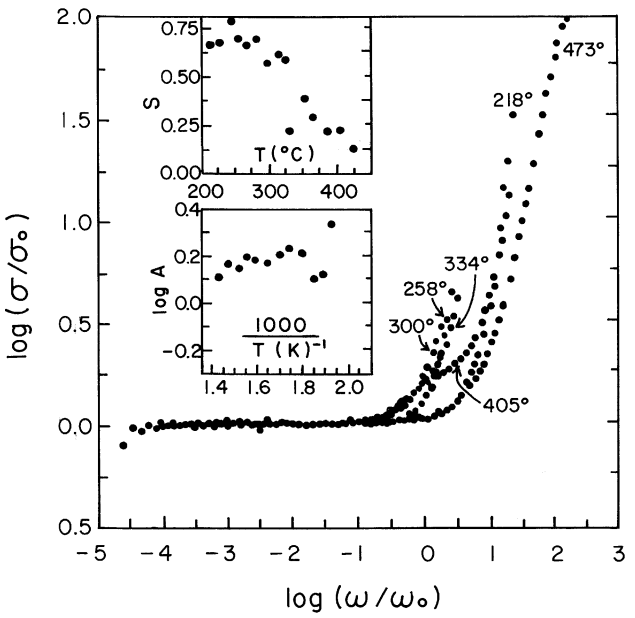

Fig. 3. Logarithmic-scaled plots of conductivity vs. frequency. These data follow the relation $\sigma/\sigma_0 = 1 + (\omega/\omega_0)^s$. The inset shows the temperature dependence of A and s. The A parameter was extracted from the universal power-law behavior, $\sigma_t(\omega) = \sigma_0 + A\omega^s$, not shown.

that was previously mentioned. Nevertheless, it is observed that in the range of temperatures studied, $\sigma_t(\omega,T)$ follows a similar trend as σ_b does.

Plots of $\log\sigma_t(\omega,T)$ vs. $\log\omega$ show that the conductivity tends to be a constant at low frequencies. There is also a frequency at which the conductivity starts to increase following a frequency power law, $\sigma_t(\omega,T) = \sigma_0 + A\omega^s$ (Jonscher's law [21]). This behavior has been observed in a wide variety of materials [22], and computed simulations [23] also predict the existence of a power law-dependent conductivity in disordered materials. In this power law, σ_0 is identified with the DC conductivity, while the term $A\omega^s$, with $s<1$, characterizes dispersive phenomena. Although A and s are temperature-dependent and the corresponding curves are not exhibited here, we have calculated both A and s parameters, and in an equivalent way, we also show $\log\{\sigma_t(\omega,T)/\sigma_0\}$ vs. $\log(\omega/\omega_0)$. These scaled plots are shown in Fig. 3. Scaling factors, σ_0 and ω_0, were determined from the $\log\sigma_t(\omega,T)$ vs. $\log\omega$ plots. This was carried out by taking the limit condition Lim $\sigma_t(\omega\to 0)\to\sigma_0$, and from the point where the curves change their slope from the frequency-independent behavior to the dispersive stage, respectively. The resultant scaled curves in Fig. 3 are properly described by the scaling law $\sigma/\sigma_0 = 1 + (\omega/\omega_0)^s$ [24], the behavior of which agree with the prediction of the jump relaxation model by Funke [25]. It must be pointed out that a master curve cannot be constructed with the scaled curves, and this fact indicates that features in the spectra do not have the same activation energy.

Bulk capacitance has been used to calculate the dielectric constant, $\varepsilon_b' = gC_b/\varepsilon_o$, where $\varepsilon_o = 8.854\times10^{-14}$ F cm^{-1}. C_b can be considered as the effective self-charging of a parallel-plate capacitor, where the film thickness determines the plate separation. Thus, ε_b' should be considered as an overall bulk characteristic. Experimental C_b values show a small (±0.4) variation as a function of temperature, and therefore ε_b' can be given as an averaged value (7.2) in the temperature range investigated.

The time-dependent response of charge movement can be given by the corresponding relaxation time, $\tau_\sigma = RC$, which was calculated from the impedance arcs. In this case, the time-dependent response lies in the interval 10^{-5}–10^{-6} s.

As mentioned in Section 1, for technological applications of these Al_2O_3 films in ACTFEL devices, the dependence on frequency of the dielectric constant, $\varepsilon'(\omega) = gC(\omega)/\varepsilon_o$, is important. Fig. 4 shows the variation of the capacitance with frequency at two selected temperatures. Although capacitance dispersion can be observed in this figure at low and high frequencies, the capacitance is almost constant with respect to the frequency and temperature over more than two decades of the frequency range analyzed. Thus, films are rather stable over quite wide intervals of temperature and frequency. An averaged value of the frequency-dependent dielectric constant is 10.6.

4. Discussion

The fact that electric response from the films can only be obtained at relatively high temperatures must be linked with the very wide energy gap (>6.2 eV)

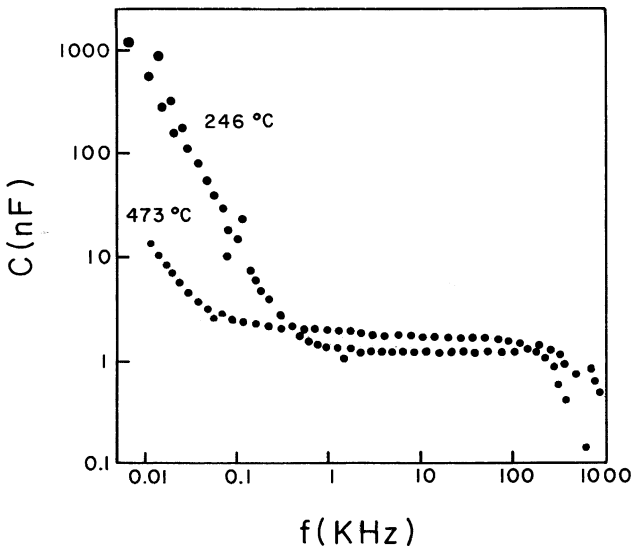

Fig. 4. Frequency dependence of the capacitance with increasing temperature.

determined [16] at room temperature for this material. We propose that the conductivity measured for the amorphous Al_2O_3 films in the present work comprises a mixture of electronic and ionic charge carriers.

4.1. Electronic contribution

Below 250 °C, most of the charge carriers are electrons tunneling from the metal Fermi-energy of electrodes into the conduction band of the Al_2O_3 film. As electrons enter the insulator, a fraction of them will be trapped in trapping states of the film, to be released later by a tunnel emission mechanism, in a similar way as that suggested by Mehta and co-workers [26,27] in the trapping behavior of the $Si/Al_2O_3/Al$ system. This is the main charge source at this stage. As is known, tunnel emission is essentially independent of temperature [28], and thus this component remains, even at high temperatures, and strongly influences the conductivity features up to 400 °C.

4.2. Ionic contribution

The common ionic charge carriers in a disordered system are cations, although anions may have appreciable mobility, particularly O^{2-}. According to the X-ray analysis [16], the Al_2O_3 films studied are considered as a three-dimensional network structure, without any long-range order, and as stated before, they are oxygen-rich materials. The probable existence of varying Al–O bond distances in the films provides a degree of structural openness, which will favor oxygen atom diffusion into the film. Assuming this possibility, it is proposed that from approximately 250 °C, an ionic component is thermally activated, with O^{2-} participating as a mobile species. Thus, O^{2-} diffusion becomes a charge carrier component of the conductivity measured. In addition, we must mention here that another characteristic of the Al_2O_3 films is that within the detection limits of the IR technique, the films are free of O–H and of Al–OH groups [16]. However, we cannot exclude the probable presence of low concentrations of these groups, which may arise from the preparation stage. If that is the case, they must necessarily contribute to the ionic activity.

There is also the possibility of an effect of proton (H^+) injection from the aluminum top electrode contributing to the AC conductivity, due to chemical reactions between the aluminum electrode and the ambient moisture, in combination with a phenomenon of field-assisted transport of ions similar to that observed in commercial soda-lime silica glass [29]. For example, a possible chemical reaction between the Al electrode and H_2O in the air that produces protons can be: $2Al + 3H_2O \rightarrow Al_2O_3 + 6H^+ + 6e^-$.

The motion of large charge carriers should be associated with dielectric loss; in Fig. 5 we show the behavior of tanδ at the selected frequencies of 100 Hz and 100 kHz in the temperature interval studied. In fact, both data sets show a relatively strong dielectric loss at approximately 250 °C, the origin of which may be attributed to the dynamic behavior of large charge carriers.

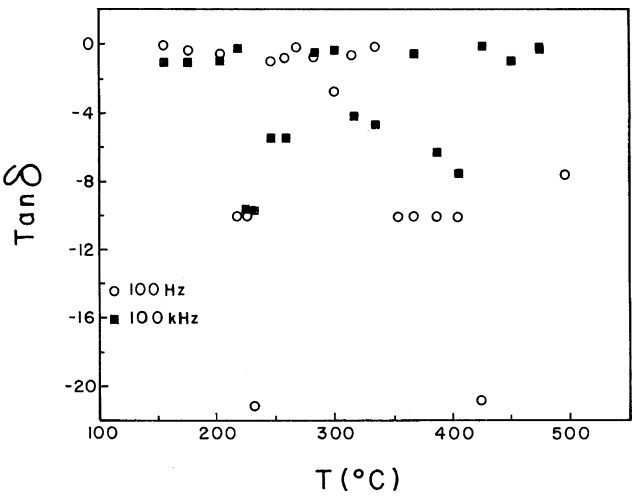

Fig. 5. Temperature dependence of the loss tangent at two selected frequencies.

Ionic mobility also promotes negative charge accumulation very close to the electrode region. The second arc on the impedance plane appears, at approximately 400°C, due to the distortion of the potential distribution in the film, caused by the accumulated spatial charge. Because of this, at the highest temperatures an incipient spike starts to develop at the low-frequency tail of the impedance curves, which is commonly [20] present for the impedance response of ionic conductors. An approximate capacitance value has a magnitude of several 100s of μF; the value can be calculated by $C \cong 1/(2\pi f Z'')$, where f and Z'' are values of the frequency and of the imaginary part of impedance in the very low-frequency region on the spike. This is a very large capacitance value, and it is characteristic of a double layer effect. Another important consequence is that the presence of the double layer inhibits the conductivity at the highest temperatures measured. This is shown in Fig. 2a,b for both $\sigma_t(\omega,T)$ and σ_b.

Above 250 °C, there are mainly two different mechanisms supporting bulk conductivity, the first one being basically non-thermally affected (electronic), and a second one arising from a diffusion mechanism (ionic). Their associated physical processes are responsible for the dielectric behavior.

The negative charge-space build-up very near the film–electrode interfaces has an associated charge transfer resistance R_2, and a capacitance C_2. Non-pronounced variation of the temperature dependence of R_2 was

observed, and thus we consider that neither R_2 nor C_2 deserve much further analysis.

Electrical resistivity values reported [30] for Al_2O_3 films deposited onto InP were 5×10^{12} Ω cm ($\sigma\cong20\times10^{-14}$ Ω^{-1} cm^{-1}) at room temperature, with an applied electric field of 10^6 V cm^{-1}. In the same work, it was also found the value of the dielectric constant increases from 8 to 10 when the frequency decreases from 1 MHz to 1 Hz. Meanwhile, Meiners [31] reported $\varepsilon'(\omega)\cong6$ at 1 MHz, and the resistivity ranged between 10^{11} and 10^{14} Ω cm at $V_g=10$ V. Metha et al. [26] report a dielectric bulk permittivity of 8.42×10^{-13} F cm^{-1}, which results in a dielectric constant of ≅9.5 for Al_2O_3 deposited on (100) silicon. By extrapolating conductivity data, we have made an approximate calculation of the conductivity at room temperature of $\cong10\times10^{-14}$ Ω cm^{-1}. We have mentioned that $\varepsilon_b'=7.2$ and $\varepsilon'(\omega)=10.6$, i.e. there is a deviation of almost 30% between the values. This difference is explained by considering that ε_b' is a parameter essentially independent of frequency, while $\varepsilon'(\omega)$ is affected by the dipolar activity associated with the ionic mobility. Therefore, values of the dielectric parameters calculated in the present work are in agreement with those for Al_2O_3 films obtained by other techniques.

The conductivity dispersion observed in Fig. 2b is attributed to relaxation phenomena. As the electrical signal varies, upward or downwards, a major or minor number of charges fail in their attempt to jump towards a new position [22], diminishing or increasing the conductivity measured. This means that forward–backward hopping is responsible for the frequency conductivity dispersion. Similar behavior of $\sigma_t(\omega,T)$ as a function of frequency and temperature have been observed in electronic and/or ionic semiconductors [32,33].

The parameter *s* has attracted attention [32], especially in relation to its physical significance. Giuntini and coworkers [33] present *s* as an evaluation of the ratio of the thermal movement of charge carriers to the energy required to trap them in their own sites. This model mainly considers a combination of mechanical and electrostatic energy, as if they were the main source of the potential energy barrier to be overcome for the charge carriers. The authors report decreasing values of *s* as temperature rises. A similar mechanism as that mentioned by these authors may be operating in the films studied. However, the parameters involved were not adjusted here.

The inset in Fig. 3 shows the behavior of *A* and *s* as a function of temperature for bulk properties only. The *A* parameter exhibits a very similar temperature dependence as the electrical conductivity does, while the temperature dependence of *s* shows a decreasing trend, similar to that observed in several glassy systems [32,33].

The second $A\omega^s$ term is present above 387 °C, the origin of which is associated with the spatial charge described before. In Fig. 3, the additional $A\omega^s$ term is observed at 405 °C. No attempt was made to calculate *A* and *s* in this last case.

5. Conclusions

The AC electrical response from amorphous Al_2O_3 films has been used to obtain dynamic, $\sigma_t(\omega,T)$, and bulk, σ_b, conductivity, as well as dielectric characteristics. Both electronic and ionic charge carriers are responsible for the total conductivity, and a hopping mechanism is involved in the charge transport process. The temperature dependence of conductivity does not exhibit linear behavior. In the temperature range studied, conductivity lies in an interval of a slightly more than two decades (10^{-6}–10^{-8}) of the logarithmic scale. The calculated dielectric constant obtained here adequately compares with that reported for amorphous Al_2O_3 films deposited by other techniques.

The results indicate that the amorphous Al_2O_3 films studied in this work are rather stable over wide ranges of frequency and temperature, which is advantageous for their technological application in ACTFEL devices.

Deviation from ideal Debye behavior should be linked with relaxation effects of polarization originating from coulombic interactions between electrons and ions with virtual charge-compensating centers. The frequency dependence of $\sigma_t(\omega,T)$ follows a classical power law [$\sigma_t(\omega,T)=\sigma_0+A\omega^s$]. To the best of our knowledge, we present here data for the *A* and *s* parameters from amorphous films for the first time. The temperature dependence of *A* follows a behavior compatible with the conductivity, while *s* decreases, as occurs in a wide variety of glass materials.

We conclude that relaxation phenomena in the Al_2O_3 films studied strongly depend on structural disorder, as in other glass substances.

Acknowledgements

The authors are indebted to Roberto de Lira Hueso and Raúl Reyes for technical assistance. We also acknowledge the financial support from DGAPA-UNAM under project IN-101799-10.

References

[1] R. Mach, G.O. Müller, Phys. Status Solidi 69 (1982) 11.
[2] A. Yoshimasha Ono, Encyclopedia of Applied Physics, 5, VCH Publishers, 1993.
[3] H. Sasakura, H. Kobayashi, S. Tanaka, J. Mita, T. Tanaka, H. Nakayama, J. Appl. Phys. 52 (1981) 6901.
[4] C.B. Thomas, W.M. Cranton, Appl. Phys. Lett. 63 (1993) 3119.

[5] S. Okamoto, E. Nakazawa, Y. Tsuchiya, Jpn. J. Appl. Phys. 29 (1990) 1987.
[6] M. García, J.C. Alonso, C. Falcony, A. Ortiz, J. Phys. D 28 (1995) 223.
[7] M. Aozasa, K. Kato, T. Nakayama, K. Ando, Jpn. J. Appl. Phys. 29 (1990) 1997.
[8] A. Ortiz, J.C. Alonso, V. Pankov, J. Mater. Sci. Mater. Electron. 10 (1999) 503.
[9] J. Ross MacDonald (Ed.), Impedance Spectroscopy, Wiley, USA, 1987.
[10] I.M. Hodge, M.D. Ingram, A.R. West, J. Electroanal. Chem. 74 (1976) 125.
[11] J.S. Bae, S.I. Pyun, J. Mater. Sci. Lett. 13 (1994) 573.
[12] R.J. Grant, A.R. West, J. Electroanal. Chem. 72 (1976) 397.
[13] F. Debuyck, L. Lemaitre, M. Moors, A.P. Van Peteghem, E. Wettinck, L. Weyten, Surf. Coat. Technol. 34 (1988) 311.
[14] J.A. González López, A. Bautista, E. Otero, X.R. Nóvoa, J. Appl. Electrochem. 29 (1999) 229.
[15] A. Ortiz, J.C. Alonso, V. Pankov, D. Albarran, J. Lumin. 81 (1999) 45.
[16] A. Ortiz, J.C. Alonso, V. Pankov, A. Huanosta, E. Andrade, Thin Solid Films 368 (2000) 74.
[17] A. Khorassani, A.R. West, Solid-State Ionics 7 (1982) 1.
[18] B.A. Buokamp, Equivalent Circuit (equiver. Pas), Department of Chemical Technology, University of Twente, Netherlands, 1988.
[19] Y. Jin, P. Dzwonkowski, J-Y. M. Eddrief, I. Riess, Solid-State Ionics 47 (1991) 137.
[20] J.T.S. Irvine, D. Sinclair, A.R. West, Adv. Mater. 2 (1990) 132.
[21] A.K. Jonscher, Nature 267 (1977) 673.
[22] A. Hunt, J. Non-Cryst. Solids 160 (1993) 183.
[23] T. Riedel, J.C. Dyre, J. Non-Cryst. Solids 172–174 (1994) 1419.
[24] D.L. Sidebottom, P.F. Grenn, R.K. Brow, J. Non-Cryst. Solids 222 (1997) 354.
[25] K. Funke, Prog. Solid-State Chem. 22 (1993) 111.
[26] D.A. Metha, S.R. Butler, F.J. Feigl, J. Electrochem. Soc. Solid-State Sci. Technol. 120 (1973) 1707.
[27] D.A. Mehta, S.R. Butler, F.J. Feigl, J. Appl. Phys. 43 (11) (1972) 4631.
[28] S.M. Sze, Physics of Semiconductor Devices, John Wiley and Sons, USA, 1981, Chapter 7.
[29] U.K. Krieger, W.A. Lanford, J. Non-Cryst. Solids 102 (1988) 50.
[30] D.C. Cameron, L.D. Irving, G.R. Jones, J. Woodward, Thin Solid Films 91 (1982) 339.
[31] L.G. Meiners, Thin Solid Films 113 (1984) 85.
[32] S.R. Elliott, F.E.G. Henn, J. Non-Cryst. Solids 116 (1990) 179.
[33] J.C. Guintini, J. Vanderschueren, J.V. Sanchetta, F. Henn, Phys. Rev. B 50 (1994) 12489.